Chemical Engineering Journal 185–186 (2012) 108–119

Contents lists available at SciVerse ScienceDirect

Chemical Engineering Journal

journal homepage: www.elsevier.com/locate/cej

Photodegradation of Orange II under visible light using Cu–Ni/TiO_2: Effect of calcination temperature

Nadia Riaz [a,*], F.K. Chong [b], Binay K. Dutta [c,1], Zakaria B. Man [a], M. Saqib Khan [a], Ela Nurlaela [a]

[a] Chemical Engineering Department, Universiti Teknologi PETRONAS, 31750 Tronoh, Malaysia
[b] Fundamental & Applied Sciences Department, Universiti Teknologi PETRONAS, 31750 Tronoh, Malaysia
[c] Chemical Engineering Department, The Petroleum Institute, Abu Dhabi, United Arab Emirates

ARTICLE INFO

Article history:
Received 11 July 2011
Received in revised form 6 January 2012
Accepted 10 January 2012

Keywords:
Cu–Ni/TiO_2
Bimetallic photocatalysts
Orange II
TiO_2 photocatalysis
Azo dyes
Transition metal doping

ABSTRACT

The decolorization of Orange II was studied under visible light using bimetallic Cu–Ni/TiO_2 prepared via precipitation method. Photocatalysts with different Cu:Ni mass compositions were prepared and the effect of calcination temperatures on the Orange II removal was investigated. The raw photocatalysts were activated by calcination at three different temperatures (180 °C, 200 °C and 300 °C) for 1 h duration. Photocatalysts were characterized using thermogravimetric analysis, Fourier-transformed infrared spectroscopy, powder X-ray diffraction and field-emission scanning electron microscopy, high resolution transmission electron microscopy, diffuse reflectance UV–Vis spectroscopy, temperature programed reduction studies and surface area analysis employing Brunauer–Emmet–Teller method. The photocatalytic degradation of Orange II was performed under the irradiation of visible light (500 W halogen lamp) at pH 6.8. The extent of Orange II degradation with initial concentration of 50 ppm was monitored using UV–Vis spectroscopy and at the end of the reaction, total organic carbon analysis (TOC) was conducted. Results from UV–Vis spectroscopy showed that high percentage of Orange II removal was achieved for Cu–Ni/TiO_2 photocatalysts calcined at 180 °C and 200 °C compared to 300 °C. In addition, these photocatalysts also displayed lower TOC values as compared to the photocatalyst calcined at 300 °C. The best performing Cu–Ni/TiO_2 photocatalyst has 9:1 Cu:Ni mass composition and calcined at 180 °C giving 100% Orange II removal with 16.1 ppm TOC value. Although the results from UV–Vis spectroscopy showed 100% Orange II removal, TOC analysis indicated the presence of organic compounds derived from the dye degradation process.

1. Introduction

The main causes of surface water and groundwater contamination are industrial discharges [1]. The textile industry has a big pollution problem. The World Bank estimates that 17–20% of industrial water pollution comes from textile dyeing and wastewater treatment. Wastewaters generated by the textile industries are known to contain considerable amounts of non-fixed dyes, especially azo-dyes, and a huge amount of inorganic salts. It has been estimated that more than 10% of the total dyestuff used in dyeing processes are released into the environment [2].

Azo dyes are the largest group of synthetic colorants used in textile industry [3] constituting 60–70% of all dyestuffs produced [4]. They have one or more azo groups (R_1—N=N—R_2) having aromatic rings mostly substituted by sulfonate group (—SO_3), hydroxyl group (—OH), etc. [5,6]. These toxic dyes are non-biodegradable and at present are abated by some common non-destructive processes [7,8].

Among azo-dyes, Orange II as shown in Fig. 1, represents more than 15% of the world production of dyes used in the textile manufacturing industry. Orange II is an anionic monoazo textile dye of the acid class. It is resistant to light degradation, the action of O_2 and common acids or bases. In wastewater treatment plants, Orange II does not undergo biological degradation [9,10]. The stability of Orange II is useful in textile manufacturing but it causes difficulty in managing its removal. Several techniques have been used to abate the model azo-dye, Orange II, such as Fenton [11], photo-Fenton [12] and TiO_2 photocatalysis [13]. However, these methods are not able to completely remove Orange II from the wastewater system using visible light. Therefore, there is a need to find a new cost effective and efficient technique to eliminate the azo-dye from industrial wastewater.

The removal of azo-dyes by advanced oxidation processes (AOPs) has been the subject of several recent studies. The mechanism of dye destruction in AOPs is based on the formation

* Corresponding author. Tel.: +60 5 368 8000; fax: +60 5 365 4075; mobile: +60 196358994.
E-mail address: nadiariazz@gmail.com (N. Riaz).
[1] Present address: West Bengal Pollution Control Board, 10A, Block III, Salt Lake, Kolkata 700 098, India.

1385-8947/$ – see front matter © 2012 Elsevier B.V. All rights reserved.
doi:10.1016/j.cej.2012.01.052

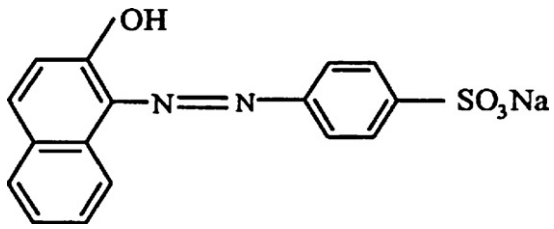

Fig. 1. Chemical structure of Orange II.

of a very reactive hydroxyl radical (•OH), that, with an oxidation potential of 2.80 V [14,15] can oxidize a broad range of organic compounds.

TiO_2 is a very suitable photocatalyst but its activity is mainly confined to the UV region of solar radiation. In order to explore efficient visible light induced photocatalysts, much scientific effort has been conducted in recent years to reduce its band gap to make it suitable for harvesting visible light from solar radiation [6]. These works include: doping TiO_2 with various transition metals such as Pt, Au, and Ag [16,17,18] non metal atoms (N, S, etc.) [19,20] and anchoring an organic dye sensitizer molecule onto the surface of the photocatalyst [9].

The use of Cu and Ni for bimetallic catalyst has been reported as the effective method to improve the efficiency of various reactions. Liu and Liu [21] and Huang and Jhao [22] reported Cu–Ni/Al_2O_3 and Ni–Cu/samaria-doped ceria catalysts for carbon dioxide hydrogenation and for steam reforming of methane, respectively. Other reported studies include decomposition of methane over Ni/SiO_2 and Ni–Cu/SiO_2 catalysts [23], Cu–Ni/TiO_2 [24] prepared via (co)impregnation with 4 wt% loading for photocatalytic reduction of nitrate; Cu–Zn/TiO_2 [25], Ni/TiO_2 [26] and Cu–Fe/TiO_2 [27] for methyl orange degradation and Cu/TiO_2 for Orange II degradation with 90% color removal in the presence of UVC light and O_2 after 150 min reaction [28].

The objective of this paper was to determine the effect of calcination temperature of the bimetallic 10 wt% Cu–Ni/TiO_2 prepared with different Cu:Ni mass compositions on the efficiency of Orange II photodegradation under visible light radiation. The goal was to remove Orange II completely using this new cost effective technique. This involved incorporation of bimetallic Cu–Ni onto TiO_2 via modified deposition–precipitation method (DP) at final pH 8.5. The introduction of Cu and Ni was with the intention to reduce the band gap of the photocatalyst for enhanced visible light absorption. The prepared photocatalysts were further characterized using thermogravimetric analysis (TGA), Fourier-transformed infrared (FTIR) spectroscopy, powder X-ray diffraction (XRD), field-emission scanning electron microscopy (FESEM), high resolution transmission electron microscopy (HRTEM), diffuse reflectance UV–Visible (DR-UV–Vis) spectroscopy, temperature programed reduction (TPR) studies and surface area analysis employing the Brunauer–Emmet–Teller method (BET).

2. Materials and methods

2.1. Materials

Copper nitrate trihydrate, $Cu(NO_3)_2{\cdot}3H_2O$ and nickel nitrate hexahydrate, $Ni(NO_3)_2{\cdot}6H_2O$ (Acros brand >98% purity) were used as dopant metal salts. Titanium dioxide, TiO_2 (Degussa P25 80% anatase, 20% rutile) was used as the support which also acts as the semiconductor in photocatalysis. Sodium hydroxide, NaOH (Merck, 95% purity) was used as precipitating agent. Glycerol used was of 95% purity (Systerm). Orange II (Acros, pure) was used as the model azo dye for photocatalytic degradation study. All chemicals were used as received.

2.2. Preparation of bimetallic photocatalyst

10 wt% Bimetallic Cu–Ni/TiO_2 photocatalysts with varying Cu:Ni mass composition were prepared via precipitation method using NaOH as precipitating agent. The monometallic 10 wt% Cu/TiO_2 and 10 wt% Ni/TiO_2 were also prepared as references. Cu and Ni salts were weighed in appropriate amount and dissolved in 100 ml of distilled water followed by the addition of glycerol in 2:1 mol ratio of glycerol:total metals with continuous stirring [29]. TiO_2 was added to the solution and stirred for 1 h. The pH of the solution was adjusted to pH 8.5 with 0.25 M NaOH. The mixture was stirred at 10 °C for 1 h before filtering and the precipitate was dried in an oven at 75 °C overnight. The dried photocatalyst was ground with a mortar and pestle, kept in air-tight glass bottle as raw photocatalyst and stored in a desiccator at room temperature prior to calcination.

2.3. Pre-treatment of photocatalysts

In order to estimate suitable calcinations temperatures for the raw photocatalysts, thermal gravimetric analysis (TGA) was carried out using Perkin Elmer (Pyris 1 TGA) instrument. The dried photocatalyst was loaded in a sample cup and weighed using a built-in microbalance attached to the instrument which automatically provide the weight of the sample (in the range of 5–10 mg). The sample was heated in flowing N_2 from 30 °C to 800 °C at a ramp rate of 20 °C/min. Results from TGA were reported as thermograms which are plots of the relative weight of the photocatalyst vs. temperature. Based on the TGA results, calcination was conducted at selected temperatures for 1 h duration. The calcined photocatalysts were given denotation: *x*Cu–*y*Ni–*T*, where '*x*' and '*y*' represent the mass composition of Cu and Ni, respectively, with '*x*' + '*y*' = 10; while '*T*' represents calcination temperature in °C.

2.4. Characterization of synthesized photocatalysts

It is important to characterize the calcined photocatalysts in order to determine their chemical and physical properties and then to relate these properties to their photocatalytic performance. In this study, photocatalysts were characterized using FTIR (Shimadzu FTIR-8400S), XRD (Bruker D8 Advance Diffractometer), FESEM (Supra55VP), HRTEM (Model: Zeiss Libra 200), DR-UV–Vis (Shimadzu), TPR (Thermo Finnigan TPDRO 1100) and BET surface area analyzer (Micromeritics ASAP 2000).

The phases present in the photocatalysts were investigated using XRD with Cu Kα radiation (40 kV, 40 mA) at 2θ angles from 10° to 80°, with a scan speed of 4° min^{-1}. The morphology of the photocatalysts such as crystallite particle shape, size, and particle size distribution were analyzed using FESEM. DR-UV–Vis measurement was performed using a UV–Vis spectrophotometer equipped with an integrating sphere. Reflectance spectrums were recorded at 190–800 nm wavelength. The band gap energies of the photocatalysts were determined from the reflectance using Kubelka–Munk function, $F(R)$, and the extrapolation of Tauc plot, which is a plot of $(F(R)\cdot h\nu)^{1/2}$ against $h\nu$. Barium sulfate (Ba_2SO_4) powder was used as a standard, an internal reference. Reflectance spectrum was collected as R-sample/R-Reference and then plotted applying Kubelka–Munk Theory in order to determine bandgap energy [32].

2.5. Photocatalytic degradation study

Photocatalytic degradation of 50 ppm Orange II was conducted using halogen lamp (500 W) as the visible light source at 25 °C with an initial solution pH 6.8. Photocatalysts with loading of 1 mg/ml

was added to 10 ml of distilled water and sonicated for 10 min in an ultrasonic bath at 25 °C followed by the addition of Orange II solution to give rise to a final concentration of 50 ppm and volume of 30 ml. The suspension was stirred using a magnetic stirrer for 2 h in the dark and later this suspension was illuminated for 1 h using 500 W halogen lamp as the visible light source at a distance of 25 cm (intensity 30856.66 lux) and the temperature of the reactor was controlled at 25 ± 2 °C by continuous cooling air. During the irradiation experiments, aliquots were withdrawn from the suspension at different intervals and immediately centrifuged to monitor the Orange II concentration and further analysis.

2.6. Orange II concentration monitoring and mineralization

The Orange II degradation during photoreaction was monitored by measuring the solution absorbance from 400 to 800 nm using a Shimadzu UV-3101 UV/Visible spectrophotometer. A calibration curve was obtained beforehand using 1, 10, 20, 30, 50 and 60 ppm standard solutions. Prior to absorbance measurement, the reaction samples were centrifuged twice at 3500 rpm for 10 min to remove the suspended solid photocatalyst. The absorbance peak at 485.0 nm was used as the representative peak for Orange II concentration [30,31]. The photodecolorization efficiency in terms of % Orange II removal was calculated as follows:

$$\%\text{Orange II removal} = \left(\frac{C_0 - C}{C_0}\right) \times 100\%$$

where 'C_0' is the initial concentration while 'C' is the concentration of Orange II at sampling time.

At the end of the reaction, total organic carbon (TOC) analysis was conducted. TOC (total organic carbon) is an important parameter to assess the organic load of wastewater which provides important information about the presence of certain organic compounds and defined as the amount of carbon bound in an organic compound. Final TOC values in ppm of the reaction samples were taken. Reaction parameters investigated were different Cu:Ni mass compositions, calcination temperatures and irradiation time. Analyses were also conducted for blank experiments where reactions were carried out: without the addition of photocatalyst, with Cu and Ni samples prepared without TiO_2 and with non-modified TiO_2.

3. Results and discussion

3.1. Pre-treatment of photocatalysts

The thermogram of the 9Cu–1Ni/TiO_2 raw photocatalyst is shown in Fig. 2. The TGA curve shows two decomposition steps between 30–180 °C and another at 180–500 °C onwards with total weight loss of 8.98%. The first step is attributed to evaporation of physically absorbed impurities and second decomposition step is attributed for decomposition of $Cu(OH)_2$ and $Ni(OH)_2$, respectively. Thus, the proposed decomposition steps for the raw photocatalysts are shown in Eqs. (1) and (2) [32].

$$Cu(OH)_2 \rightarrow CuO_{(s)} + H_2O_{(g)} \quad (1)$$

$$Ni(OH)_2 \rightarrow NiO_{(s)} + H_2O_{(g)} \quad (2)$$

Thermograms of the other raw photocatalysts (not shown) with different Cu:Ni mass compositions are similar to that displayed in Fig. 2. Based on the thermogram, three calcination temperatures were selected: 180 °C, 200 °C and 300 °C, for a duration of 1 h.

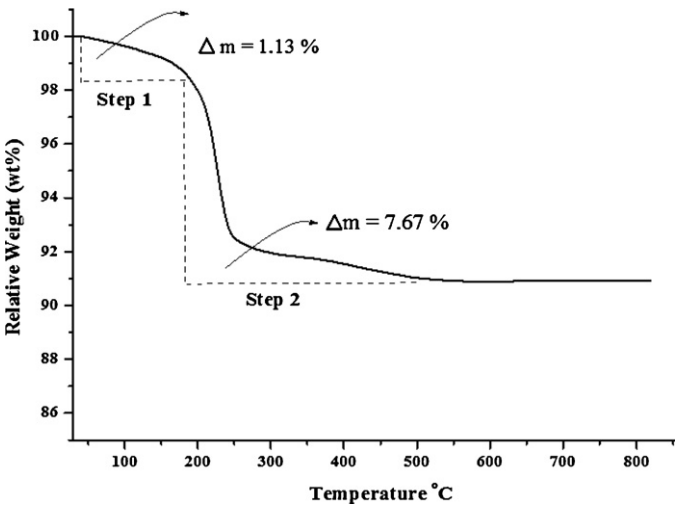

Fig. 2. Thermogram of 9Cu–1Ni/TiO_2 raw photocatalyst.

3.2. Characterization

3.2.1. Fourier-transformed infrared (FTIR) spectroscopy

Fig. 3 shows the FTIR spectra of the raw and calcined 9Cu–1Ni/TiO_2 photocatalysts. Several absorption peaks are observed. The broad band around 3400 cm^{-1} is attributed to O–H stretching, and the peak near 1600 cm^{-1} to O–H bending which is related to physically absorbed moisture. The IR band observed from 400 to 900 cm^{-1} corresponds to the Ti–O stretching vibrations [32,33]. The band at 1382 cm^{-1} attributed to nitrate (NO_3^-) group, is present in both raw and calcined photocatalysts even after calcining at 300 °C. Similar band at 1384 cm^{-1} was also observed by Li and Inui [34] referred to nitrate which is always present when nitrate salts are used as precursors. No evidence of the presence of Si–OH contamination (sharp band at 3635 cm^{-1}) in FTIR spectra is observed [35].

3.2.2. XRD

The XRD patterns of bare TiO_2 and Cu–Ni/TiO_2 photocatalysts calcined at 200 °C with different Cu:Ni mass compositions are presented in Fig. 4(a). On the other hand, the XRD patterns for Cu–Ni/TiO_2 photocatalysts with 9:1 Cu:Ni mass composition

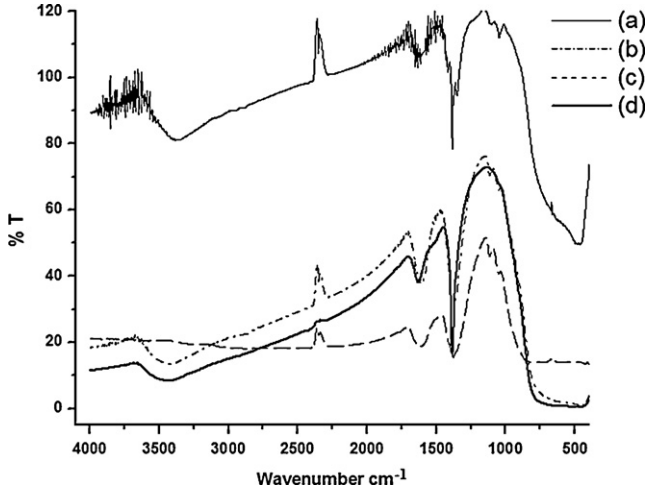

Fig. 3. FTIR spectra of 9Cu–1Ni/TiO_2 photocatalysts: raw (a); and calcined at 180 °C (b), 200 °C (c) and 300 °C (d).

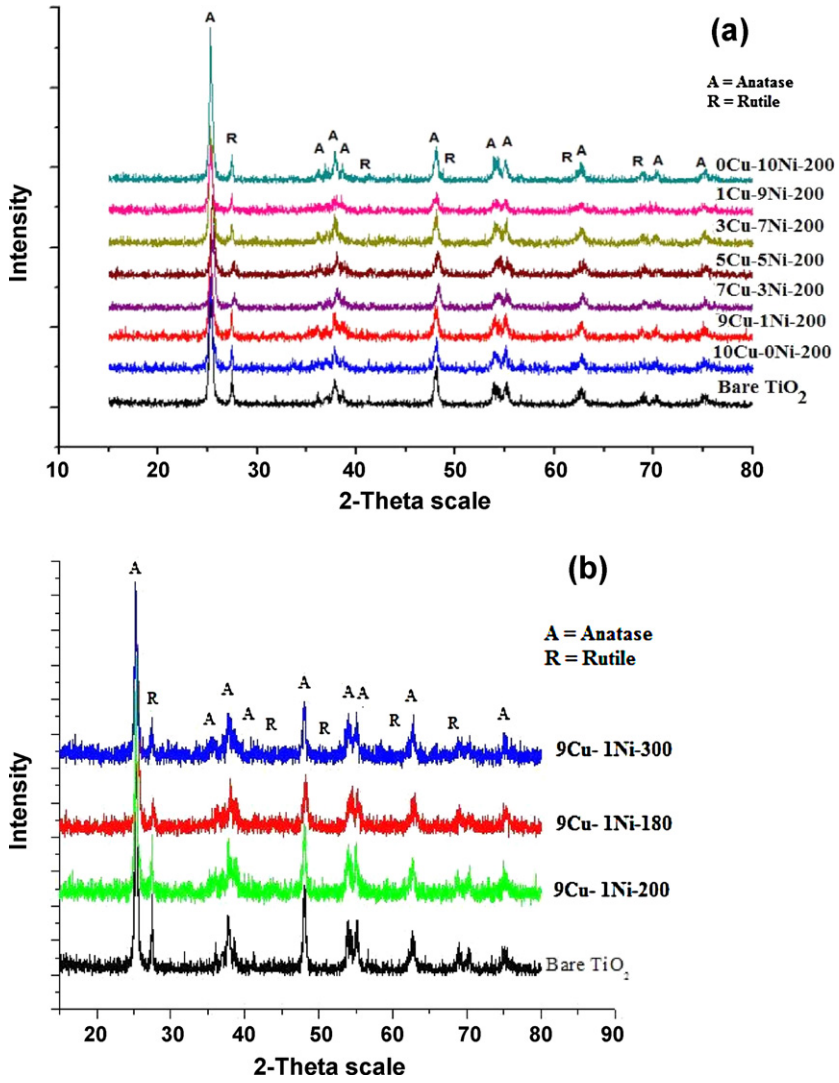

Fig. 4. XRD patterns of bare TiO_2 and Cu–Ni/TiO_2 with (a) different Cu:Ni mass compositions calcined at 200 °C and (b) Cu:Ni mass composition 9:1 calcined at different temperatures (A, anatase, R, rutile).

calcined at different temperatures are shown in Fig. 4(b). No significant differences were detectable for the XRD patterns for all the samples. The main peaks at $2\theta = 25.34^\circ$ and 27.46° corresponded to anatase and rutile phases, respectively [32,36,37,38] were present for bare TiO_2 and all the photocatalysts. No phase transition from anatase to rutile was observed for all the calcined photocatalysts, neither the presence of diffraction lines for Cu–and Ni–containing phases. This may indicate high metallic dispersion [39]. Zhu et al. [40] reported that characteristic peaks of metal oxide phase could only be visible when the metal dopant concentration on TiO_2 was above 5 wt%. However, for this paper, at 10 wt% metal loading, the absence of Cu, Ni or mixed Cu–Ni oxide phases clearly indicated that the dopants were well dispersed on TiO_2. This may be due to the use of glycerol during photocatalyst preparation that favored the formation of small metal particles since it has been reported that glycerol prohibited the aggregation of metal particles [41].

3.3. Photocatalyst morphology: FESEM and HRTEM

Morphology of the photocatalyst often plays important role in its catalytic properties. The particle size has an important influence on the photocatalytic process due to changes in transmission, dispersion and absorption of light, and in the catalyst surface availability. The FESEM micrographs of the prepared photocatalysts with different Cu:Ni mass compositions as shown in Fig. 5, clearly depict uniform distribution with irregular sized spherical morphologies with slight agglomeration ranging from 11 to 35 nm. Yoong et al. [32] and Nurlaela et al. [39,42] also reported similar results of agglomeration for Cu/TiO_2.The degree of agglomeration for the photocatalyst with Cu:Ni mass composition 9:1 was higher when calcined at 300 °C when compared to that calcined at 200 °C. This may be due to sintering during calcination process [42]. It was observed from EDX mapping (Fig. 5b) of the photocatalysts that the dopant metals were uniformly dispersed onto the support. These findings are in agreement with the XRD results indicating that the doped metals were well dispersed onto the support.

In this work, HRTEM was used to obtain more detailed discernable microstructure information in order for single grains and grain boundaries to be accurately analyzed. The Cu–Ni/TiO_2 photocatalysts samples calcined at 200 °C and bare TiO_2 were analyzed using HRTEM to obtain crystallite size and morphology. As shown in Fig. 6, the HRTEM micrographs display very good crystalline morphology of the particles with irregular morphology. The size of the particles were in the range of 11–30 nm for Cu–Ni/TiO_2 and 11–35 nm for bare TiO_2. Results are in good agreement with the FESEM data in terms of the metal particles morphology.

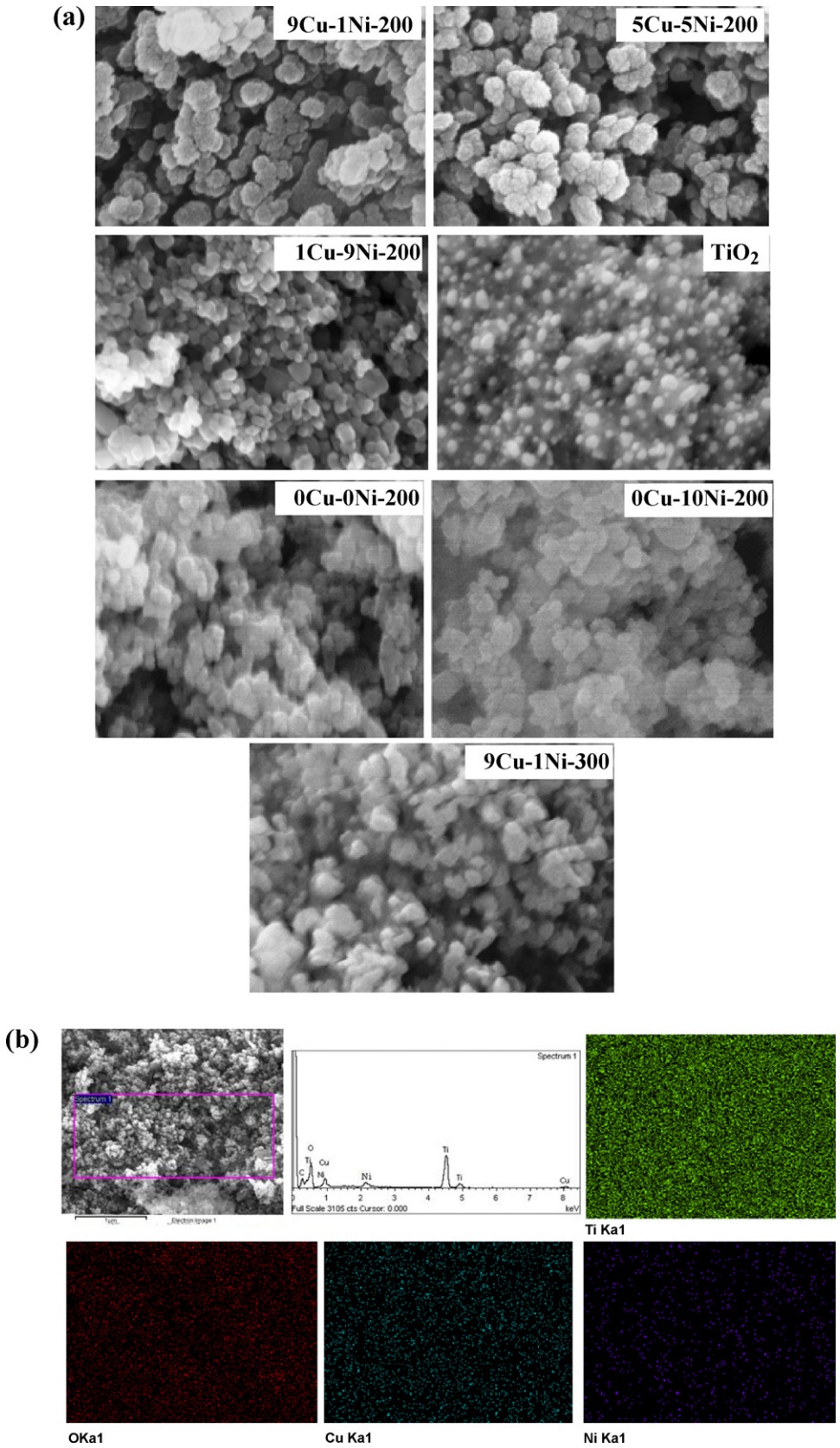

Fig. 5. (a) FESEM micrographs of bare TiO_2, Cu–Ni/TiO_2 with different Cu:Ni mass compositions calcined at 200 °C and 9Cu–1Ni mass composition calcined at 300 °C (150k×). (b) EDX and Mapping image of 9Cu–1Ni/TiO_2 photocatalysts.

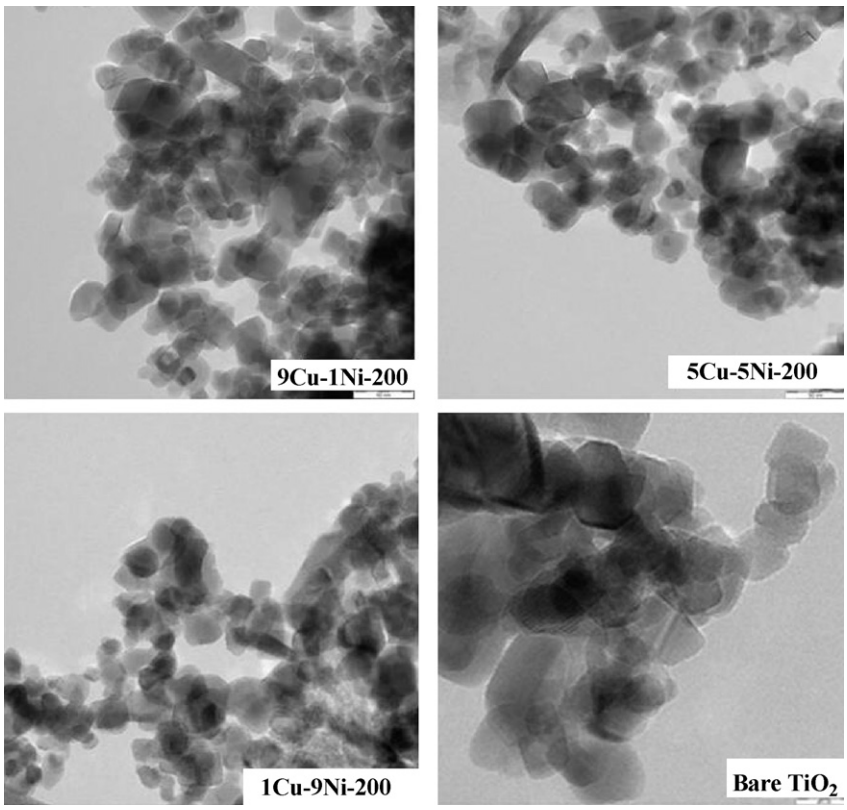

Fig. 6. HRTEM micrographs of bare TiO_2 and Cu–Ni/TiO_2 with different Cu:Ni mass compositions calcined at 200 °C (50 nm).

3.3.1. Diffuse reflectance UV–Visible (DR-UV–Vis) spectroscopy

One of the challenges in the development of TiO_2 is to shift the absorption spectrum of TiO_2 into the visible region to enable more efficient sunlight harvesting. In this work, incorporation of bimetallic Cu–Ni onto TiO_2 was chosen for this purpose. In order to determine the band gap energy of the photocatalysts, DR-UV–Vis was conducted. The DR-UV–Vis spectra of bare TiO_2 and Cu–Ni/TiO_2 photocatalysts with different Cu:Ni mass compositions are presented in Fig. 7. DR-UV–Vis spectrum of bare TiO_2 showed absorption peaks ranging from 190 nm and 400 nm, similar to that observed by Yoong et al. [32] and Nurlaela et al. [39]. The absorption at 323 nm is generally related to the electronic excitation from O 2p valence band to Ti 3d conduction band indicating that Ti presents as tetrahedral Ti^{4+} species [43]. The activities of the prepared photocatalysts as compared to bare TiO_2 are presented in Table 1. The light absorption properties of TiO_2 modified with Cu–Ni was enhanced significantly. The band gap energies of the photocatalysts (Fig. 8) were determined from the Tauc plot, a plot of $(F(R)\cdot h\nu)^{1/2}$ against $h\nu$. $F(R)$ is the Kubelka–Munk function derived from reflectance spectra where $F(R) = (1-R)^2/2R$ equation, and $h\nu$ is the photon energy.

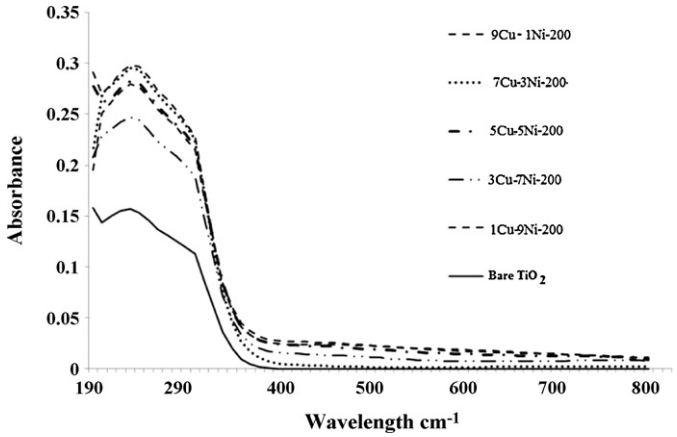

Fig. 7. Absorption spectra of bare TiO_2 and Cu–Ni/TiO_2 calcined at 200 °C with different Cu:Ni mass compositions.

3.3.2. Temperature programed reduction (TPR)

The TPR profiles of the photocatalysts are presented in Fig. 9. TPR was employed to characterize the Cu–Ni/TiO_2 photocatalyst with respect to the type of metal oxide species present, either copper oxide, nickel oxide, or copper–nickel mixed oxide, and the degree of interaction of the oxides with TiO_2 support [32]. The reduction profile of bimetallic photocatalyst with 9:1 and 1:9 Cu–Ni mass compositions showed similar reduction peaks at 294 °C while for 5Cu–5N–200 reduction peaks was at 308 °C with a shoulder around 444 °C.

The reduction profile of Cu–Ni/TiO_2 calcined at 200 °C with 9:1 and 1:9 Cu:Ni mass compositions displayed reduction peak at 294 °C correlating to reduction of CuO with strong interaction with TiO_2 [44] or might be attributed to the reduction of Cu–Ni

Table 1
Calculated band gap energies of bare TiO_2 and Cu–Ni/TiO_2 photocatalysts.

Photocatalyst	Bandgap energy (eV)	% Orange II removal	TOC
Bare TiO_2	3.16	21	55.7
10Cu–0Ni–200	2.90	54.9	19.1
9Cu–1Ni–200	3.0	100	20.2
7 Cu–3Ni–200	3.1	63	18.8
5Cu–5Ni–200	3.0	100	21.9
3Cu–7Ni–200	3.0	97.3	23.2
1Cu–9Ni–200	2.97	90.4	27.8
0Cu–10Ni–200	3.14	46.7	25.2

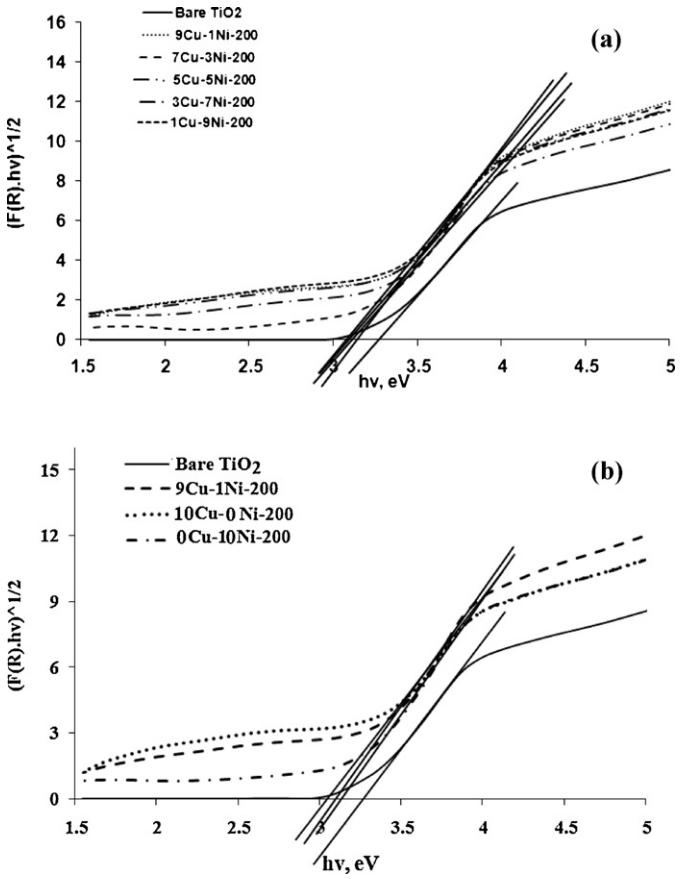

Fig. 8. (a) and (b) Plot of transformed Kubelka–Munk functions $[F(R) \cdot h\nu]^{1/2}$ vs. $h\nu$ for bare TiO_2 and Cu–Ni/TiO_2 calcined at 200 °C with different Cu:Ni mass compositions.

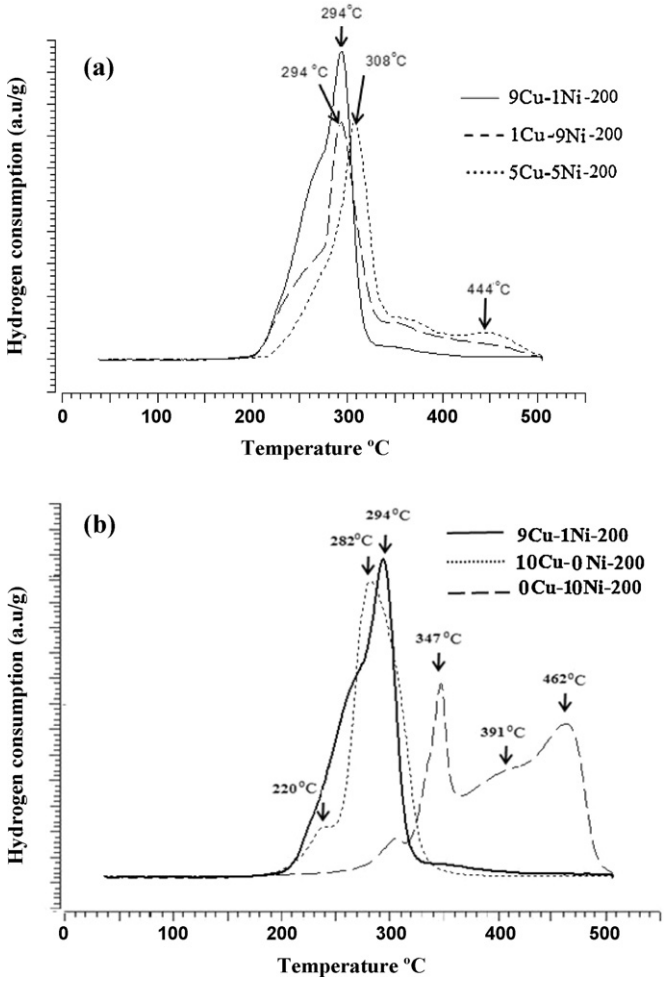

Fig. 9. The TPR profiles of (a) Cu–Ni/TiO_2 photocatalysts with different Cu:Ni mass compositions calcined at 200 °C and (b) 10 wt% monometallic and bimetallic Cu–Ni/TiO_2 photocatalysts calcined at 200 °C.

mixed oxide instead of individual oxide. It is observed that the reduction peak and shoulder for CuO are shifted to higher temperature. The small shoulders below 250 °C might be attributed to the reduction of highly dispersed CuO with less interaction with the TiO_2 support [32,45] and also correspond to Cu(II) reduction to Cu(0) [46]. Apparently, smaller CuO particles were formed on the surface of photocatalyst, decreasing the reduction temperature. The 5Cu–5Ni–200 displayed a peak at 308 °C attributed to the reduction of NiO having strong interaction with TiO_2 [47]. The weaker shoulder at 444 °C corresponded to the well dispersed NiO with weak metal–support interaction [42]. With respect to the different Cu:Ni mass compositions only small differences were observed. In Fig. 9(b), reduction peaks can be easily differentiated for the monometallic Cu/TiO_2 and Ni/TiO_2 photocatalysts calcined at 200 °C, with 282 °C for bulk CuO, 347 °C and 462 °C for bulk NiO.

3.3.3. The surface area of photocatalyst

The BET surface area, pore volume, and pore diameter of bare TiO_2 and Cu–Ni/TiO_2 photocatalysts with different Cu:Ni mass compositions are shown in Table 2. All the samples displayed Type IV isotherms with hysteresis loops, which indicates capillary condensation in mesoporous adsorbate [48,49,32,39]. TiO_2 displayed type III pattern, which is typically ascribed to non-porous products with weak interactions between the adsorbent and the adsorbate. With reference to the effect of Cu:Ni mass compositions on surface area, all the supported bimetallic photocatalysts have specific surface area of ~43 $m^2\ g^{-1}$. However, no clear trend could be deduced for the total surface area of the photocatalysts. The surface area increased with Cu content but at high Ni loading, a decrease in surface area was observed. Average pore diameter increased with the increase in Ni contents and decrease of Cu contents.

In case of calcination temperature, the surface area and pore volume increased with calcination temperature while the pore diameter of photocatalyst decreased with increasing temperature as shown in Table 2. However, the BET surface area reached the maximum (51.8 $m^2\ g^{-1}$) for photocatalyst with 5:5 Cu:Ni mass composition calcined at 300 °C. High metal dispersion on the TiO_2 surface was reported when the total surface area of photocatalysts was increased [42]. With reference to the degradation reaction study as shown in Fig. 10(a), the results of photocatalyst with 5Cu:5Ni mass composition calcined at 200 °C (with the highest BET surface area) displayed almost similar performance in terms of TOC results as compared to Cu:Ni; 9:1 and 1:9 photocatalysts,

Table 2
The BET surface area of bare TiO_2 and Cu–Ni/TiO_2 photocatalyst.

Photocatalyst	BET surface area ($m^2\ g^{-1}$)	Total pore volume ($cm^{-3}\ g^{-1}$)	Average pore diameter (nm)
Bare TiO_2	43.1	0.20	18.5
9Cu–1Ni–180	42.5	0.29	27.7
9Cu–1Ni–200	43.2	0.21	19.5
9Cu–1Ni–300	49.9	0.28	22.6
5Cu–5Ni–180	45.4	0.29	25.9
5Cu–5Ni–200	45.6	0.38	33.7
5Cu–5Ni–300	51.8	0.28	21.7
1Cu–9Ni–200	43.4	0.36	33.9

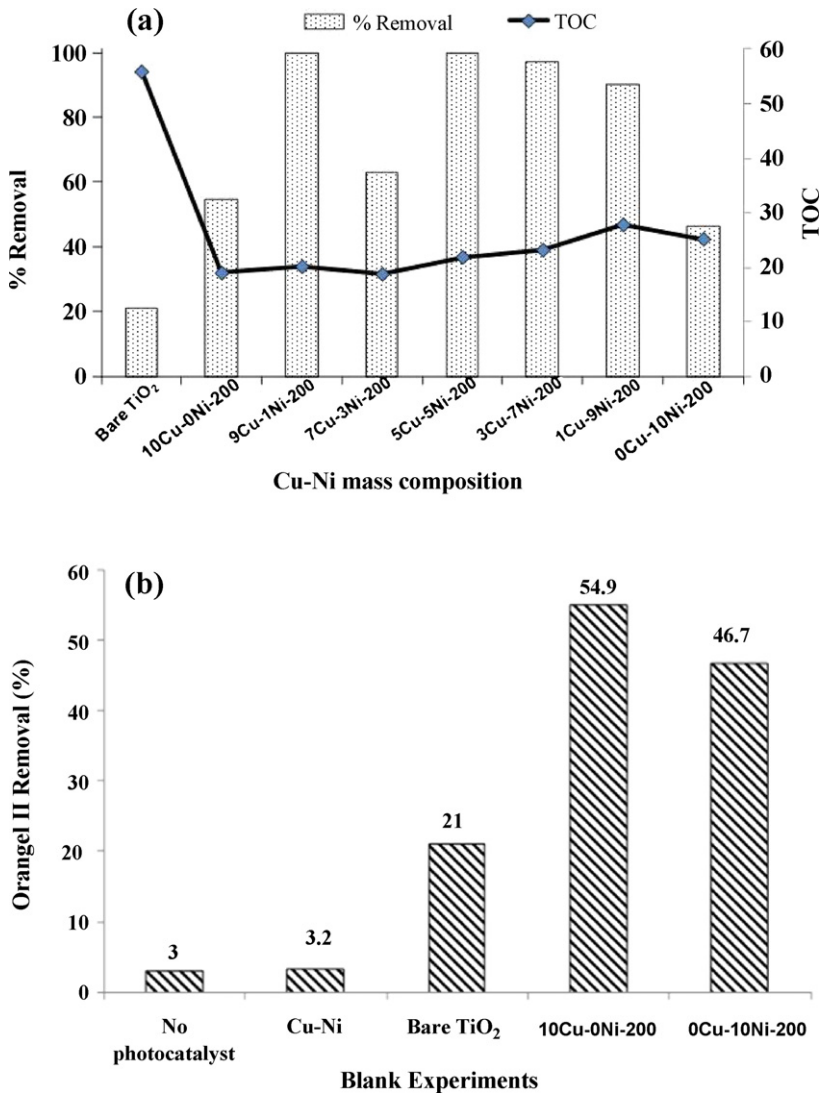

Fig. 10. (a) Photocatalytic degradation of Orange II using bare TiO_2 and Cu–Ni/TiO_2 photocatalysts with different Cu–Ni mass compositions. (b) Photocatalytic degradation of Orange II using Cu–Ni, bare TiO_2, Cu/TiO_2, Ni/TiO_2 photocatalysts and Orange II solution without TiO_2.

indicating that surface area may not be the major factor responsible for the photocatalytic activity.

3.4. Orange II concentration monitoring and mineralization

3.4.1. Effect of Cu:Ni mass composition

Results from the effect of different Cu:Ni mass compositions on Orange II degradation are presented in Fig. 10(a), (b) and Table 3. Photocatalysts calcined at 200 °C showed 100% dye removal for Cu:Ni mass compositions of 9:1 and 5:5 as shown in Fig. 10(a). However, photocatalysts with 3:7 Cu:Ni mass composition showed 97.3% Orange II removal. In the case of photocatalysts with 7:3 and 1:9 Cu:Ni mass composition, lower dye removal activity was observed compared to the other photocatalysts with different Cu:Ni mass compositions. The degradation activity decreased further to 90.4% and 63.0% for photocatalysts with 1:9 and 7:3 mass compositions, respectively.

At lower calcination temperature (180 °C), the photocatalysts displayed better activity with 100% Orange II removal for photocatalysts with 9:1, 5:5 and 1:9 Cu:Ni mass compositions (Table 3). For photocatalyst with 3:7 Cu:Ni mass composition, it showed higher activity (93.3%) compared to that with 7:3 Cu:Ni mass composition (75.2%). For the photocatalysts calcined at 300 °C, the Orange

Table 3
Removal of Orange II and TOC values.

Cu:Ni ratio	Cal. temperature	% Removal	TOC (ppm)
(9:1)	180	100.0	16.1
(7:3)	180	75.2	20.2
(5:5)	180	100.0	64.7
(3:7)	180	93.3	22.5
(1:9)	180	100.0	26.1
(9:1)	200	100.0	20.2
(7:3)	200	63.0	18.8
(5:5)	200	100.0	21.9
(3:7)	200	97.3	23.2
(1:9)	200	90.4	27.8
(9:1)	300	57.1	45.8
(7:3)	300	76.0	42.1
(5:5)	300	72.0	44.2
(3:7)	300	58.0	43.6
(1:9)	300	66.5	42.3
(10:0)	200	54.9	19.1
(0:10)	200	46.7	25.2
Bare TiO_2	–	21	55.7
Cu–Ni	200	3.2	–
No photocatalyst	–	3.0	36.7

TOC, total organic carbon.

II removal was in the range of 57.1–76.0%, the highest displayed by photocatalyst with 7:3 Cu:Ni mass composition.

In terms of dye mineralization, only photocatalysts with 100% Orange II removal were taken into consideration. Even though results from UV–Vis spectroscopy showed complete Orange II removal, TOC analysis registered the presence of organic compounds which were derived from the dye degradation process. For 200 °C calcination temperature (Fig. 10(a)), photocatalysts with 9:1 and 5:5 Cu:Ni mass compositions displayed TOC values of 20.2 ppm and 21.9 ppm, respectively. The photocatalysts calcined at 180 °C which showed complete removal of Orange II were those with 9:1, 5:5 and 1:9 Cu:Ni mass compositions, and the displayed TOC values were 16.1 ppm, 64.7 ppm and 26.1 ppm, respectively. Monometallic 10 wt% Cu/TiO_2 and 10 wt% Ni/TiO_2 photocatalysts with 10:0 and 0:10 Cu:Ni mass compositions, respectively, displayed much lower activity compared to the bimetallic catalysts but showed higher Orange II removal compared to bare TiO_2. Furthermore, activity of monometallic Cu/TiO_2 (54.9%) was reported with better performance compared to and Ni/TiO_2 (46.7%). Therefore, the presence of bimetallic Cu–Ni displayed synergistic effect for dye removal. Results with improved activity for TiO_2 doped with Cu and Ni, were reported for Cu–Ni/TiO_2 [42] for hydrogen production and Ni*x*Cu*y*/Al_2O_3 [50], methanol steam reforming, photocatalytic reduction of nitrate [24], Orange II degradation [51,52] with respect to the monometallic ones.

Blank experiments were also conducted for comparison purposes. Orange II solution (50 ppm) without the addition of any photocatalyst (No photocatalyst) with the addition of TiO_2 (Bare TiO_2) was chosen for blank experiments. The bimetallic Cu–Ni prepared in the same conditions as for the Cu–Ni/TiO_2 photocatalysts but in the absence of TiO_2 (Cu–Ni) was also considered. The activities of these samples were compared with the monometallic 10 wt% Cu/TiO_2 (10Cu–0Ni–200) and 10 wt% Ni/TiO_2 (0Cu–10Ni–200) photocatalysts in Fig. 10(b). Bare TiO_2, monometallic 10 wt% Cu/TiO_2 and 10 wt% Ni/TiO_2 photocatalysts displayed 21.0%, 54.9% and 46.7%, respectively, of Orange II % removal. However, in the absence of TiO_2, Orange II removal was negligible, giving 3.0% and 3.2%, for "No photocatalyst" and Cu–Ni, respectively. This indicates that the active material for photodegradation of Orange II is TiO_2 and bimetallic Cu–Ni acts as modifier to reduce the band gap of TiO_2 [42].

In the present study, compared to monometallic Cu/TiO_2 and Ni/TiO_2 photocatalysts, Bimetallic Cu–Ni/TiO_2 photocatalysts showed better photocatalytic activity in terms of Orange II % removal as shown in Table 3. Furthermore, activity of monometallic photocatalysts in terms of Orange II degradation, Cu/TiO_2 (54.9%) was reported with better performance compared to and Ni/TiO_2 (46.7%). These results conform to the previous studies reported for the enhanced photoactivity for the bimetallic Cu–Ni/TiO_2 photocatalyst by Gao et al. [24], Nurlaela et al. [39], Riaz et al. [51] and Riaz et al. [52].

Changes in the catalytic properties induced by adding Cu to Ni is caused by changes in the electronic properties of the homogeneous alloy particle, by the formation of active surface structures, by preferential segregation of one metal to the surface or by a combination of all these effects [22,53,54]. The catalytic properties of bimetallic nanoparticles are directly related to their structure and composition which may be controlled by processes taking place during catalyst preparation [55]. For example, even though Cu has a lower surface free energy than Ni and should, based on thermodynamics, preferentially occupy surface sites [56], core–shell structures with Ni surface enrichment [53] or Cu surface enrichment [54] does occur. For a tiny metal-modified semiconductor particle, supported bimetal Cu and Ni can behave as short-circuited photoelectrochemical cell, where both cathodic and anodic reactions can occur on the same particle [57]. For photogenerated electrons and holes, metal Ni and Cu in the semiconductor surface can separately trap these reductive electrons and oxidative holes and prevent their combinations, then transfer these trapped electrons or holes to absorbed substances in their surface, thereby increase their existent life and improve the efficiency of a photocatalytic reaction. It has also been reported that the Cu^{2+} doped TiO_2 catalyst increased the photocatalytic degradation of two typical azo dyes used in dyeing industry namely Orange II and Tartrazine (Tart) [58]. The behavior of Cu^{2+} was explained on the basis that Cu^{2+} may scavenge electrons resulting in the formation of Cu^{+}, which in turn enhances the oxidation of the substrate [59].

In the present research, XRD patterns, Fig. 4(a) and (b) of Cu–Ni/TiO_2 photocatalyst showed only the main characteristic peaks of TiO_2 support, no phase transition from Anatase to rutile and characteristic reflections for Ni, Cu or their Cu–Ni combination (alloy) containing phases are observed. These results were further confirmed by FESEM analysis which indicates that metal particles are well dispersed or interact with TiO_2 support. The interaction with the support and the concomitant presence of the two metals strongly promoted the reducibility of the material [50]. Previously it was also reported that the catalytic performance of bimetallic systems was promising in the methanol stream reforming [50] and reduction of nitrate into nitrite [24]. The Introduction of copper in the catalyst formulation showed excellent performance and furthermore this promoting effect of bimetal is probably attributed to the more effective separation of photogenerated spatial charges in tiny TiO_2 semiconductor particles [24].

3.4.2. Effect of calcination temperature

10 wt% Bimetallic Cu–Ni/TiO_2 photocatalysts calcined at three different temperatures (180, 200 and 300 °C with calcination duration 1 h) is studied for Orange II degradation. High percentage removal of Orange II is observable using Cu–Ni/TiO_2 calcined at 180 °C and 200 °C in the range 63–100% giving TOC values of 16.1 ppm to 64.7 ppm, after 1 h of reaction (Table 3). At higher calcination temperature (300 °C), lower performance is observed from 57.1% to 76% dye removal with 42.1–45.2 ppm TOC values. The reaction using TiO_2 standard displayed the lowest Orange II removal (21%) with very high TOC value (55.7 ppm).

Photocatalysts calcined at 180 °C and 200 °C showed 100% Orange II removal for 9:1 Cu:Ni mass compositions with 16.1 and 20.2 ppm TOC value. For the 9:1 Cu:Ni mass composition, at higher calcination temperature (300 °C), lower dye degradation was observed with only 57.1% Orange II removal and 45.2 ppm TOC value.

3.4.3. Effect of irradiation time

Fig. 11 displayed the % Orange II removal as a function of time (120 min dark reaction followed by 60 min light reaction) for photocatalysts with 9:1 Cu:Ni mass composition. During dark reaction, decolorization was the fastest for photocatalyst calcined at 180 °C compared to the other temperatures. It was already 100% after 60 min in the dark without exposure to irradiation indicating high dye adsorption rate. For photocatalyst calcined at 200 °C, Orange II removal was observed even in the dark, and the removal progressed to 85.5% after 120 min in the dark. The degradation progressed further to 100% after 60 min irradiation. However, for photocatalyst calcined at 300 °C and bare TiO_2, degradation rate was very slow (40.0%) compared to other two photocatalysts. It is evident that the percentage of decolorization and photodegradation increases with irradiation time for photocatalysts calcined at 200 °C and 300 °C. Photocatalysts calcined at 300 °C showed less adsorption during dark reaction but the rate of reaction during irradiation was comparable to that for photocatalyst calcined at 200 °C. The reaction rate during light reaction decreases with irradiation time as it follows the pseudo first-order kinetics and additionally a competition

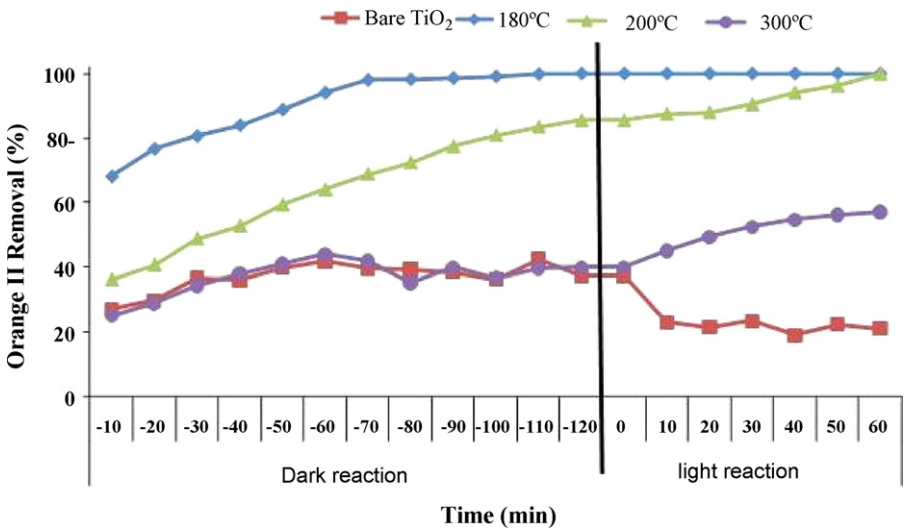

Fig. 11. Orange II degradation in the dark and with radiation using photocatalysts with 9:1 Cu:Ni mass composition calcined at different temperatures.

for degradation may occur between the reactant and the intermediate products. The slow kinetics of dye degradation after certain time limit is mainly attributed to: (a) the difficulty in converting the N-atoms in Orange II into oxidized nitrogen compounds [60], (b) the slow reaction of short chain aliphatics with •OH radicals [61] and (c) the short life-time of photocatalyst because of active sites deactivation by strong by-products deposition (carbon, etc.) [62].

Photocatalysis is a surface phenomenon, a critical step in intervening in the effectiveness of photodegradation is adsorption of pollutants on the photocatalyst surface [63]. Many workers measured the adsorption and the kinetics of photodegradation of different compounds on TiO_2 photocatalyst, such as phenol [64] and Methylene Blue [65], 2-chlorophenol [66], Reactive Black [65,67] and monoazo dye (Reactive Red 198), poliazo dye (Direct Green 99) [63] and supported TiO_2 catalyst for Orange II [68].

In all the cited studies, organic compounds are adsorbed on the photocatalyst surface to some degree. The adsorption process proceeds to reach an equilibrium and then lamps are switched on and the photocatalysis process is conducted. In the case of dyes, there may be some problems to distinguish the adsorption of dyes on the photocatalyst surface from the photocatalytic decomposition of the dyes. There is no problem if the adsorption of the dye on the surface of TiO_2 is negligible [69,70].

A comparison study was performed using bare TiO_2 and Cu–Ni/TiO_2 separately, which showed overall removal of Orange II by Cu–Ni/TiO_2 photocatalysts was considerably higher than that of bare TiO_2. All the experiments were performed under natural pH condition (pH 6.8) using 50 ppm of Orange II, and 1 mg l^{-1} of photocatalyst dose. The dark adsorption experiments involving all photocatalysts indicate that effective surface area (Table 2) and adsorption capacity of the synthesized Cu–Ni/TiO_2 were much higher than bare TiO_2, which favor rapid removal of Orange II from the solution.

Although all the supported catalysts showed very good adsorption characteristics compared to that of bare TiO_2, pure support (bare TiO_2) with surface area 43.1 m^2 g^{-1} showed very poor adsorption of Orange II. Orange II being slightly acidic and anionic is subjected to electrostatic repulsion and the negative surface of the support.

4. Conclusion

Bimetallic Cu–Ni/TiO_2 photocatalysts were prepared with different Cu:Ni mass compositions and calcined at different temperatures. In the present work, Cu–Ni/TiO_2 photocatalysts displayed better photocatalytic activity of as high as 100% Orange II removal as compared to bare TiO_2 which displayed only 21.0%. The XRD patterns of the bimetallic photocatalysts did not show the presence of separate metal diffraction peaks for Cu or Ni phases. This is mainly due to the high metal dispersion of the metals onto TiO_2. Results from the XRD and FESEM analyses were in favor to the metal particles existing in the form of well dispersed oxides on TiO_2.

The reduction profile (TPR) of bimetallic photocatalyst showed similar reduction peaks indicating the presence of Cu and Ni mixed oxides. Surface area of photocatalysts was almost similar to the bare $TiO_2 \sim 43$ m^2 g^{-1} except for 5:5 Cu–Ni ratio, observed with higher surface area. The photocatalyst performance of the bimetallic system is promising compared to bare TiO_2 and the monometallic photocatalysts. Decolorization was faster for 180 °C compared to other calcination temperatures which may be due to the increased pore diameter. The best performing Cu–Ni/TiO_2 photocatalyst has 9:1 Cu:Ni mass composition and calcined at 180 °C giving 100% Orange II removal with 16.1 ppm TOC value. Although the results from UV–Vis spectroscopy showed 100% Orange II removal, TOC analysis indicated the presence of organic compounds derived from the dye degradation process.

Acknowledgment

The authors would like to acknowledge Universiti Teknologi PETRONAS for the funding of this research work.

Appendix A. Supplementary data

Supplementary data associated with this article can be found, in the online version, at doi:10.1016/j.cej.2012.01.052.

References

[1] M.N. Rashed, A.A. El-Amin, Photocatalytic degradation of methyl orange in aqueous TiO_2 under different solar irradiation sources, International Journal of Physical Sciences 2 (2007) 073–081.
[2] R.J. Maguire, Occurrence and persistence of dyes in Canadian river, Water Science and Technology 26 (1992) 265–270.
[3] S. Meric, D. Kaptan, T. Olmez, Color and COD removal from wastewater containing reactive black 5 using Fenton's oxidation process, Chemosphere 54 (2004) 435–441.

[4] C.M. Carliell, S.J. Barclay, C.A. Buckley, Microbial decolourization of a reactive azo dye under anaerobic conditions, in: Water Research Commission South Africa, 1995, pp. 61–69.
[5] C. O'Neill, A. Lopez, S. Esteves, F.R. Hawkes, D.L. Hawkes, S. Wilcox, Azo-dye degradation in an anaerobic–aerobic treatment system operating on simulated textile effluent, Applied Microbiology and Biotechnology 53 (2000) 249–254.
[6] P. Rajaguru, K. Kalaiselvi, M. Palanivel, V. Subburam, Biodegradation of azo dyes in a sequential anaerobic–aerobic system, Applied Microbiology and Biotechnology 54 (2000) 268–273.
[7] A. Reife, H. Freeman, Environmental Chemistry of Dyes and Pigments, Wiley/Interscience, New York, NY, 1996.
[8] M.R. Hoffmann, S.T. Martin, W. Choi, D.W. Bahnemann, Environmental applications of semiconductor photocatalysis, Chemical Reviews 95 (1995) 69–96.
[9] G. Helz, R. Zepp, D. Crosby, Aquatic and Surface Chemistry, Lewis Publishers, Boca Raton, FL, 1995.
[10] M. Halmann, Photodegradation of Water Pollutants, CRC Press, Boca Raton, FL, 1996.
[11] C. Morrison, J. Bandara, J. Kiwi, Sunlight induced decoloration/degradation of non-biodegradable Orange II dye by advanced oxidation technologies is homogeneous and heterogeneous media, Journal of Advanced Oxidation Technologies 1 (1996) 160–169.
[12] F. Herrera, A. Lopez, J. Kiwi, Photochemically activated degradation of reactive dyes: statistical modeling of the reactor performance, Journal of Photochemistry and Photobiology A: Chemistry 135 (2000) 45–51.
[13] D.F. Ollis, H. Al-Ekabi, Photocatalytic Purification and Treatment of Water and Air, Elsevier, Amsterdam, 1993.
[14] O. Legrini, E. Oliveros, A.M. Braun, Photochemical processes for water treatment, Chemical Reviews 93 (1993) 671–698.
[15] S.-F. Kang, C.-H. Liao, S.-T. Po, Decolorization of textile wastewater by photo-fenton oxidation technology, Chemosphere 41 (2000) 1287–1294.
[16] M. Anpo, M. Takeuchi, The design and development of highly reactive titanium oxide photocatalysts operating under visible light irradiation, Journal of Catalysis 216 (2003) 505–516.
[17] F. Bosc, A. Ayral, N. Keller, V. Keller, Room temperature visible light oxidation of CO by high surface area rutile TiO_2 supported metal photocatalyst, Applied Catalysis B 69 (2007) 133–137.
[18] H. Kisch, L. Zang, C. Lange, W.F. Maier, C. Antonius, D. Meissner, Modified, amorphous titania – a hybrid semiconductor for detoxification and current generation by visible light, Angewandte Chemie International Edition 37 (1998) 3034–3036.
[19] Y.C. Hong, C.U. Bang, D.H. Shin, H.S. Uhm, Band gap narrowing of TiO_2 by nitrogen doping in atmospheric microwave plasma, Chemical Physics Letters 413 (2005) 454–457.
[20] G. Tian, K. Pan, H. Fu, L. Jing, W. Zhou, Enhanced photocatalytic activity of S-doped TiO_2–ZrO_2 nanoparticles under visible-light irradiation, Journal of Hazardous Materials 166 (2009) 939–944.
[21] Y. Liu, D. Liu, Study of bimetallic Cu–Ni/γ-Al_2O_3 catalysts for carbon dioxide hydrogenation, International Journal of Hydrogen Energy 24 (1999) 351–354.
[22] T.-J. Huang, S.-Y. Jhao, Ni–Cu/samaria-doped ceria catalysts for steam reforming of methane in the presence of carbon dioxide, Applied Catalysis A: General 302 (2006) 325–332.
[23] M.J. Lázaro, Y. Echegoyen, I. Suelves, J.M. Palacios, R. Moliner, Decomposition of methane over Ni–SiO_2 and Ni–Cu–SiO_2 catalysts: effect of catalyst preparation method, Applied Catalysis A: General 329 (2007) 22–29.
[24] W. Gao, R. Jin, J. Chen, X. Guan, H. Zeng, F. Zhang, N. Guan, Titania-supported bimetallic catalysts for photocatalytic reduction of nitrate, Catalysis Today 90 (2004) 331–336.
[25] D. Zhang, F. Zeng, Photocatalytic oxidation of organic dyes with visible-light-driven codoped TiO_2 photocatalysts, Russian Journal of Physical Chemistry A, Focus on Chemistry 85 (2011) 1077–1083.
[26] D. Zhang, Chemical synthesis of Ni/TiO_2 nanophotocatalyst for UV/visible light assisted degradation of organic dye in aqueous solution, Journal of Sol–Gel Science and Technology 58 (2011) 312–318.
[27] D. Zhang, Enhanced photocatalytic activity for titanium dioxide by co-modification with copper and iron, Transition Metal Chemistry 35 (2010) 933–938.
[28] R.S.K. Wong, J. Feng, X. Hu, P.L. Yue, Discoloration and mineralization of non-biodegradable azo dye Orange II by copper-doped TiO_2 nanocatalysts, Journal of Environmental Science and Health Part A: Toxichazardous Substances Environmental Engineering 39 (2005) 2583–2595.
[29] K.A. Crouse, M. Badri, H.A. Hassan, F.K. Chong, Copper–glycerol complex isolation and characterization, in: PORIM International Palm Oil Congress (Chemistry & Technology), PIPOC, 1996, pp. 233–237.
[30] K. Bourikas, C. Kordulis, A. Lycourghiotis, Differential potentiometric titration: development of a methodology for determining the point of zero charge of metal (hydr)oxides by one titration curve, Environmental Science & Technology 39 (2005) 4100–4108.
[31] Y. Zhiyong, E. Mielczarski, J. Mielczarski, D. Laub, P. Buffat, U. Klehm, P. Albers, K. Lee, A. Kulik, L. Kiwi-Minsker, A. Renken, J. Kiwi, Preparation, stabilization and characterization of TiO_2 on thin polyethylene films (LDPE). Photocatalytic applications, Water Research 41 (2007) 862–874.
[32] L.S. Yoong, F.K. Chong, B.K. Dutta, Development of copper-doped TiO2 photocatalyst for hydrogen production under visible light, Energy 34 (2009) 1652–1661.
[33] X. Yan, J. He, D.G. Evans, Y. Zhu, X. Duan, Preparation, characterization and photocatalytic activity of TiO_2 formed from mesoporous precursor, Journal of Porous Materials 11 (2004) 131–139.
[34] J.L. Li, T. Inui, Characterization of precursors of methanol synthesis catalysts, copper/zinc/aluminum oxides, precipitated at different pHs and temperatures, Applied Catalysis A: General 137 (1996) 105–117.
[35] Greg W. GrHflth., Quantitation of silanol in silicones by FTI R spectroscopy, Industrial & Engineering Chemistry Product Research and Development 23 (1984) 590–593.
[36] A. Bauer, K. Lee, C. Song, Y. Xie, J. Zhang, R. Hui, Pt nanoparticles deposited on TiO_2 based nanofibers: electrochemical stability and oxygen reduction activity, Journal of Power Sources 195 (2010) 3105–3110.
[37] M. Xie, L. Jing, J. Zhou, J. Lin, H. Fu, Synthesis of nanocrystalline anatase TiO_2 by one-pot two-phase separated hydrolysis-solvothermal processes and its high activity for photocatalytic degradation of rhodamine B, Journal of Hazardous Materials 176 (2010) 139–145.
[38] T. Sreethawong, Y. Suzuki, S. Yoshikawa, Photocatalytic evolution of hydrogen over mesoporous TiO_2 supported NiO photocatalyst prepared by single-step sol-gel process with surfactant template, International Journal of Hydrogen Energy 30 (2005) 1053–1062.
[39] E. Nurlaela, F.K. Chong, B.K. Dutta, N. Riaz, Bimetallic Cu–Ni/TiO_2 as photocatalyst for hydrogen production from water, in: International Conference on Fundamental and Applied Sciences (ICFAS2010), 15–17 June, 2010.
[40] H. Zhu, Y. Wu, X. Zhao, H. Wan, L. Yang, J. Hong, Q. Yu, L. Dong, Y. Chen, C. Jian, J. Wei, P. Xu, Influence of impregnation times on the dispersion of CuO on anatase, Journal of Molecular Catalysis A: Chemical 243 (2006) 24–30.
[41] Y. Li, M. Cai, J. Rogers, Y. Xu, W. Shen, Glycerol-mediated synthesis of Ni and Ni/NiO core–shell nanoparticles, Materials Letters 60 (2006) 750–753.
[42] E. Nurlaela, Development of Cu–Ni/TiO_2 Bimetallic Catalyst For Photohydrogen Production under Visible Light Illumination, Masters Thesis, Universiti Teknologi PETRONAS, Tronoh, Bandar Seri Iskandar, 2011.
[43] M.D. Fuerte, Hernández-Alonso, A.J. Maira, A. Martínez-Arias, M. Fernández-García, J.C. Conesa, J. Soria, G. Munuera, Nanosize Ti–W mixed oxides: effect of doping level in the photocatalytic degradation of toluene using sunlight-type excitation, Journal of Catalysis 212 (2002) 1–9.
[44] M.D. Romero, J.A. Calles, A. Rodríguez, Influence of the preparation method and metal precursor compound on the bifunctional Ni/HZSM-5 catalysts, Industrial & Engineering Chemistry Research 36 (1997) 3533–3540.
[45] L. Millard, M. Bowker, Photocatalytic water–gas shift reaction at ambient temperature, Journal of Photochemistry and Photobiology A: Chemistry 148 (2002) 91–95.
[46] M.J. Lázaro, Y. Echegoyen, C. Alegre, I. Suelves, R. Moliner, J.M. Palacios, TiO_2 as textural promoter on high loaded Ni catalysts for methane decomposition, International Journal of Hydrogen Energy 33 (2008) 3320–3329.
[47] M.D. Romero, J.A. Calles, A. Rodríguez, J.C. Cabanelas, The influence of calcination treatment over bifunctional Ni/HZSM-5 catalysts, Industrial & Engineering Chemistry Research 37 (1998) 3846–3852.
[48] S. Rahimnejad, S.S. Rahman, M.R. Gholami, A credible role of copper oxide on structure of nanocrystalline mesoporous titanium dioxide, Journal of Iranian Chemical Society 5 (2008) 367–374.
[49] K.S.W. Sing, D.H. Everett, R.A.W. Haul, L. Moscou, R.A. Pierotti, J. Rouquerol, T. Siemieniewska, Reporting physisorption data for gas/solid systems with special reference to the determination of surface area and porosity, Pure & Applied Chemistry 57 (1985) 603–619.
[50] D. Rogatis, Loredana, T. Montini, B. Lorenzut, P. Fornasiero, NixCu/Al_2O_3 based catalysts for hydrogen production, Energy & Environmental Science 1 (2008) 501–509.
[51] N. Riaz, F.K. Chong, B.K. Dutta, M.S. Khan, E. Nurlaela, Photocatalytic degradation of Orange II using bimetallic Cu–Ni/TiO_2 photocatalysts, in: International Conference on Fundamental and Applied Sciences (ICFAS2010), Convention Centre, Kuala Lumpur, 2010.
[52] N. Riaz, F.K. Chong, B.K. Dutta, M.S. Khan, E. Nurlaela, Effect of photocatalysts preparation methods and light source on Orange II photocatalytic degradation, in: 2nd International Conference on Environmental Science and Technology, vol. 6, Singapore, IPCBEE, 2011, pp. 111–117.
[53] S. Wu, C. Zhu, W. Huang, Properties of polymer supported Ni–Cu bimetallic catalysts prepared by solvated metal atom impregnation, Chinese Journal of Polymer Science 14 (1996) 217–224.
[54] H. Wang, R.T.K. Baker, Decomposition of methane over a Ni–Cu–MgO catalyst to produce hydrogen and carbon nanofibers, Journal of Physical Chemistry B 108 (2004) 20273–20277.
[55] P. Li, J. Liu, N. Nag, P.A. Crozier, In situ preparation of Ni–Cu/TiO_2 bimetallic catalysts, Journal of Catalysis 262 (2009) 73–82.
[56] J.H. Sinfelt, Catalysis by alloys and bimetallic clusters, Accounts of Chemical Research 10 (1977) 15–20.
[57] K.T. Ranjit, T.K. Varadarajan, B. Viswannathan, Photocatalytic reduction of nitrite and nitrate ions over oxide (ZnO, ZrO_2 and Fe_2O_3) semiconductors, Indian Journal of Chemistry Section A: Inorganic Bio-Inorganic Physical Theoretical & Analytical Chemistry 35 (1996) 177–181.
[58] K.V.S. Rao, B. Lavédrine, P. Boule, Influence of metallic species on TiO_2 for the photocatalytic degradation of dyes and dye intermediates, Journal of Photochemistry and Photobiology A: Chemistry 154 (2003) 189–193.
[59] M.A. Rauf, M.A. Hisaindee, S. Meetani, An overview on the photocatalytic degradation of azo dyes in the presence of TiO_2 doped with selective transition metals, Desalination 276 (2011) 13–27.

[60] J. Bandara, V. Nadtochenko, J. Kiwi, C. Pulgarin, Dynamics of oxidant addition as a parameter in the modelling of dye mineralization (Orange II) via advanced oxidation technologies, Water Science and Technology 35 (1997) 87–93.
[61] C. Walling, Fenton's reagent revisited, Accounts of Chemical Research 8 (1975) 125–131.
[62] Y. Li, S. Sun, M. Ma, Y. Ouyang, W. Yan, Kinetic study and model of the photocatalytic degradation of rhodamine B (RhB) by a TiO_2-coated activated carbon catalyst: effects of initial RhB content, light intensity and TiO_2 content in the catalyst, Chemical Engineering Journal 142 (2008) 147–155.
[63] M. Janus, E. Kusiak-Nejman, A.W. Morawski, Determination of the photocatalytic activity of TiO_2 with high adsorption capacity, Reaction Kinetics, Mechanisms and Catalysis 103 (2011) 279–288.
[64] B. Serrano, M. Salaices, A. Ortiz, H.I. de Lasa, Quasi equilibrium and non equilibrium adsorption in heterogeneous photocatalysis, Chemical Engineering Science 62 (2007) 5160–5166.
[65] B. Tryba, A.W. Morawski, T. Tsumura, M. Toyoda, M. Inagaki, Hybridization of adsorptivity with photocatalytic activity—carbon-coated anatase, Journal of Photochemistry and Photobiology A: Chemistry 167 (2004) 127–135.
[66] I. Ilisz, A. Dombi, K. Mogyorósi, A. Farkas, I. Dékány, Removal of 2-chlorophenol from water by adsorption combined with TiO_2 photocatalysis, Applied Catalysis B: Environmental 39 (2002) 247–256.
[67] A. Aguedach, S. Brosillon, J. Morvan, E.K. Lhadi, Influence of ionic strength in the adsorption and during photocatalysis of reactive black 5 azo dye on TiO_2 coated on non woven paper with SiO_2 as a binder, Journal of Hazardous Materials 150 (2008) 250–256.
[68] A. Bhattacharyya, S. Kawi, M.B. Ray, Photocatalytic degradation of Orange II by TiO_2 catalysts supported on adsorbents, Catalysis Today 98 (2004) 431–439.
[69] C.L. urković, D. Ljubas, H.C. Juretić, L. urković, D. Ljubas, H. Juretić, Photocatalytix decolorization kinetics of diazo dye Congo Red aqueous solution by UV/TiO_2 nanoparticles, Reaction Kinetics, Mechanisms and Catalysis 99 (2010) 201–208.
[70] Y. Zhu, S. Xu, D. Yi, Photocatalytic degradation of methyl orange using polythiophene/titanium dioxide composites, Reactive and Functional Polymers 70 (2010) 282–287.